Electronic Supplementary Material (ESI) for Polymer Chemistry.

Supplementary Information

Predictive Design of Multimonomeric Polyelectrolytes Enables Lung-Specific Gene Delivery

Jeffrey M. Ting,[*a] John D. Fisher,[a] Tyler Conyers,[a] Suteja Patil,[a] Catherine G. Robohn,[a] Teresa Tamayo-Mendoza,[a] Felipe Oviedo,[a] Shashi K. Murthy[a]

[a] Nanite, Inc., Boston, Massachusetts 02109

1. Materials and Methods 2
2. Reactivity Ratio Determination 7
3. Polymer Characterization 10
4. Dynamic Light Scattering Analysis 12
5. qPCR Detailed Methodology and Tissue Analysis 18
6. *In Vitro* Transfection Evaluation 21
7. References 23

1. Materials and Methods

Materials. Unless otherwise stated, the following materials were used as received: N-(3-aminopropyl)methacrylamide hydrochloride (APMAm, >98%, Polysciences), 2-(trimethylammonio)ethyl methacrylate chloride (TMAEMA, , Sigma), and 3-phenoxy-2-hydroxypropyl methacrylate (PhHPMA, >95%, Polysciences), 4-((((2-carboxyethyl)thio)carbonothioyl)thio)-4-cyanopentanoic acid (CTA1, 95%, Boron Molecular), poly(ethylene glycol) 4-cyano-4-(phenylcarbonothioylthio)pentanoate (CTA2, Mn 2000 g/mol, Sigma), 2,2'-Azobis[2-(2-imidazolin-2-yl)propane]dihydrochloride (VA-044, Fujifilm Wako Chemicals USA), Methoxy-poly(ethylene glycol)-block-poly(L-lysine hydrochloride) (mPEG2K-b-PLKC100, Alamanda Polymers), acetic acid (AA, glacial, ≥99.7%, Sigma), hydrochloric acid solution (HCl, 6N, Sigma), methanol (MeOH, HPLC, 99.9%, Fisher), sodium chloride solution (5 M, X), calcium chloride (CaCl2, anhydrous ≥96.0%, Sigma), glucose (2 g/L, X), aluminum oxide (activated, basic, Brockmann I), SnakeSkin dialysis tubing (MWCO 3.5K, 22 mm, Thermo Fisher Scientific). All water was dispensed from a Milli-Q water purification system filtered at a resistivity of 18.2 MΩ-cm at 25 °C. Plasmid DNA (pDNA, pCMV-EGFP, 3657 bp) was purchased from VectorBuilder (Chicago, IL, USA). In vivo-jetPEI® was purchased from Polyplus and used as instructed.

Automated Synthesis Details. Polymers P1 to P3 were prepared from high-throughput synthesis runs using an Opentron OT-2 equipped with P300 and P1000 pipettes. All monomers were passed through an aluminium oxide column prior to use and prepared in 3.5 M stock solutions. Liquid handling calibrations and accurate aspiration of viscous monomer stock solutions were accounted for using standard Opentron protocols. In general, to 4 mL glass vials in 24-well plates, pre-calculated volumes of monomer, initiator, chain transfer agent, and solvent (1.5 M total

monomer) were transferred. Stir bars were added before sealing the vials for sparging with inert anhydrous nitrogen gas for 20 min. Vials were then individually moved to a StarFish PolyBlocks Workstation (Heidolph, USA) for well-mixed heating at 60 °C. RAFT reactions were quenched by cooling to room temperature and exposure to air with the addition of 1 mL of 6 N HCl. Low volume aliquots of the crude sample were purified by gel filtration column and lyophilized for 2 days to afford light yellow free-flowing solid polymer.

Manual Synthesis Details. Polymers P4 to P6 were prepared manually in an analogous manner as described above in the "Automated Synthesis Details" section, except that chemicals were transferred directly by hand to 20 mL glass vials. All monomers were passed through an aluminium oxide column prior to use. Crude samples were purified completely by dialysis against 4 L Milli-Q water for 2 days with at least 3 exchanges of the dialysate before lyophilization for 3 days to afford light pink free-flowing solid polymer.

Size-exclusion chromatography (SEC). SEC measurements were conducted on Tosoh EcoSEC Elite GPC System equipped with two TSKgel columns (G3000PWXL-CP and G5000PWXL-CP) with pore sizes suitable for samples with effective molecular weights from 200-50,000 and 400-500,000 g/mol, respectively, and the TSKgel SuperH-RC reference column. The SEC is equipped with a temperature- controlled dual-flow Refractive Index (RI) Detector and a UV-8420 Detector. All SEC measurements were collected at a flow rate of 1 mL/min relative to PEG standards purchased from PSS (ReadyCal Kit PEG/PEO, M_n 238, 2070, 14900, 196000 g/mol). Samples were dissolved in the mobile phase at 5 mg/mL and filtered through PES 0.22 um filters before SEC analysis. Chromatograms were analyzed using the EcoSEC Elite workstation software.

^{1}H NMR Spectroscopy. Proton NMR measurements were collected using a JEOL 400 MHz NMR with a Royalprobe with 16 scans and 4 s relaxation delay. NMR spectra were processed and analyzed using iNMR (Version 6.4.5).

Polyplex Preparation. Polymer stock solutions were prepared in 4 mL glass vials by direct dissolution of polymer in filtered Milli-Q water at 75 mM (expressed as nitrogen residues) total concentration. These samples were vortexed for at least 30 s and allowed to equilibrate at room temperature for at least 30 min prior to use. PNP assemblies were prepared by mixing diluted polymer stock solutions with 250 ng pDNA stock solutions at specific N/P ratios in order of DNA, salt/sugar additive, then polymer in this order before equilibration.

Automated Dynamic Light Scattering (DLS). Polyplexes were prepared with pDNA at N/P ratio of 5 under various solution conditions (see Dynamic Light Scattering Analysis section below). They were incubated at room temperature for at least 45 min before DLS measurement. An automated DynaPro® Plate Reader III (Wyatt Instruments, CA, USA) was used to collect 5 acquisitions per well in duplicate. With the DYNAMICS software (Wyatt Instruments, CA, USA), autocorrelation functions were processed using an automated baseline filtering, and the polyplex size distributions were calculated using both a cumulant fit (ISO 22412 and ASTM 2490-09 algorithms) and regularization (non-negative least squares fitting algorithm). The apparent mean hydrodynamic radius (R_h) values are reported from at least three repeated measurements.

Animal Work. The *in vivo* animal work for this study was performed by Biomere Biomedical Research Models, Inc. (Worcester, MA, USA) following a standard protocol of lateral tail vein injections for gene delivery applications in mouse models. All animal work was carried out in accordance with NIH Office of Laboratory Animal Welfare (OLAW) and Association for Assessment and Accreditation of Laboratory Animal Care (AAALAC) assurance. Briefly, 5-7

week-old female BALB/c mice were subject to intravenous injection of 200 µL prepared PNP working solution containing 5 µg of a 3.7 kb CMV-EGFP pDNA construct, monitored over time, and sacrificed after 6 h. Animals were intracardially perfused with PBS to remove blood before tissue collection and tissues were flash frozen and stored at -80 °C until processing.

Quantitative Real-time PCR (qPCR). Tissue DNA extraction was performed with a DNeasy Blood & Tissue Kit (Qiagen, MD, USA). Custom TaqMan qPCR forward primers, reverse primers, and probes with specificity to EGFP (GTCCGCCCTGAGCAAAGA, TCCAGCAGGACCATGTGATC, and CCCAACGAGAAGCG) or mouse ß-actin (AGGCTGTGCTGTCCCTGTATG, CCCGTCTCCGGAGTCCAT, and CTCTGGTCGTACCACAGG) were designed to quantify the relative delivery of EGFP-containing pDNA to each mouse organ. qPCR was run with TaqMan™ Fast Advanced Master Mix for qPCR (Thermo Fisher Scientific, Waltham, MA, USA) on a QuantStudio 7 Pro Real-Time PCR System (Thermo Fisher Scientific, Waltham, MA, USA) and analyzed using the $-\Delta\Delta C_T$ method. Three technical replicates were done for each qPCR. The average ΔC_T values for a PBS-only injection were used as a control injection to calculate $-\Delta\Delta C_T$ values.

In Vitro Transfection Experiments. HEK293T cells were grown in DMEM media supplemented with 10% fetal bovine serum and Penicillin-Streptomycin. Cells were maintained in a humidified incubator (Thermo Forma Direct Heat CO_2 Incubator) set to 5% CO_2 and 37 °C. Approximately 24 h before transfection, 7,500 HEK293T cells (in DMEM media supplemented with 10% fetal bovine serum) were seeded in each well of a poly-L-Lysine coated 96 well plate. PNPs were complexed with 250 ng of pCMV-EGFP in PBS for 45 min and then 50 µL of solution was added dropwise to each well. After 72 h, cells were stained with Hoechst 33342, media was replaced with FluoroBrite DMEM supplemented with GlutaMAX, and imaged.

High-Content Cellular Imaging and Analysis. Live-cell *in vitro* images were collected with high-throughput confocal imaging (PerkinElmer Operetta CLS). The imaging plate was loaded into the Operetta and visualized using Harmony software to adjust the wells, stacks, and thresholds of the nuclei, GFP, and cytoplasm cell channels identified by different markers. The images were uploaded to a cloud storage where 96 folders representing the 96-well plate were uploaded, and TIFF images were stored for every channel, stack, and frame inside each folder. The raw images were then downloaded using Python and further processed to reproduce them as seen on the Operetta and quantified to evaluate efficiency and viability metrics using machine learning.

For each frame in a well folder, the images were categorized into separate channels and z-stacked across planes. Channels of each stacked plane were considered for maximum intensity projection to create a RGB image of the frame. The images were transformed into a shape of Tensor: ([1,3,1080,1080]), indicating an image with three color channels (RGB) and a resolution of 1080 x 1080 pixels. MEDIAR-Former,[1] a cell segmentation tool, was used on each image to predict a binary mask for nuclei and cytoplasm cells. The total number of nuclei cells in the image was calculated as the total cells in the binary mask of the nuclei channel and total alive cells were calculated as the cells in binary mask of cytoplasm channel that are present in the same position as the cells in binary mask of nuclei channel. The total GFP cells in the image were determined by the intersection of positions of the GFP cells in the original image and alive cells in the binary mask. Metrics were calculated as follows:

$$Efficiency = \frac{Total\ GFP\ Cells}{Total\ Nuclei\ Cells}$$

$$Viability = \frac{Total\ Alive\ Cells}{Average\ of\ Total\ Alive\ Cells\ in\ Negative\ Control\ Wells}$$

2. Reactivity Ratio Determination

Pairwise reactivity ratio values were determined from free radical polymerizations using VA-044 as an initiator in deuterated acetic acid and deuterated methanol (3:1 *v*/*v*) with 0.05% TMS as an internal standard at 60 °C. Targeted feed monomer fractions were 0.25 (Run 1), 0.50 (Run 2), and 0.75 (Run 3) for each monomer combination. The initiator molar concentration was fixed at 1000 times less than the total monomer concentration. After manually transferring monomer (1 M), initiator, and 1 mL solvent to a dried 4 mL glass vial, the reaction vial was seal and sparged with anhydrous nitrogen for 20 min. An aliquot was directly transferred to an NMR tube for analysis of the crude starting material. Samples were moved to a hot plate set at 60 °C for ~4 min before quenching to an ice bath and opening to air, so that the total monomer conversion was targeted to be around 15% or lower to minimize effects of compositional drift on reactivity.

Fig. S-1 shows a representative ^{1}H NMR spectrum of the crude starting material of the APMAm and TMAEMA copolymerization reaction, used to determine the actual feed ratio between monomers. Total monomer conversion was determined by comparing the monomer vinyl proton at 5.1 ppm to the internal standard proton at 1.2 ppm between the crude starting material and the crude 4 min spectra. The initial (actual) feed ratio of monomers was determined from the ^{1}H NMR spectrum of the starting material. Fig. S-2 shows representative ^{1}H NMR spectra for the targeted 0.5 monomer fraction (Run 2) for APMAm/TMAEMA, TMAEMA/PhHPMA, and PhHPMA/APMAm terminated at 4 min without purification.

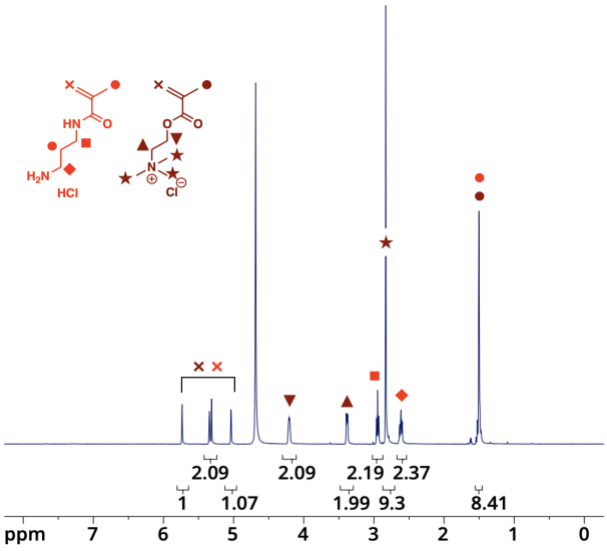

Figure S-1. ^{1}H NMR of the starting material of APMAm and TMAEMA in acetic acid-d4 and methanol-d4 (3:1 *v*/*v*).

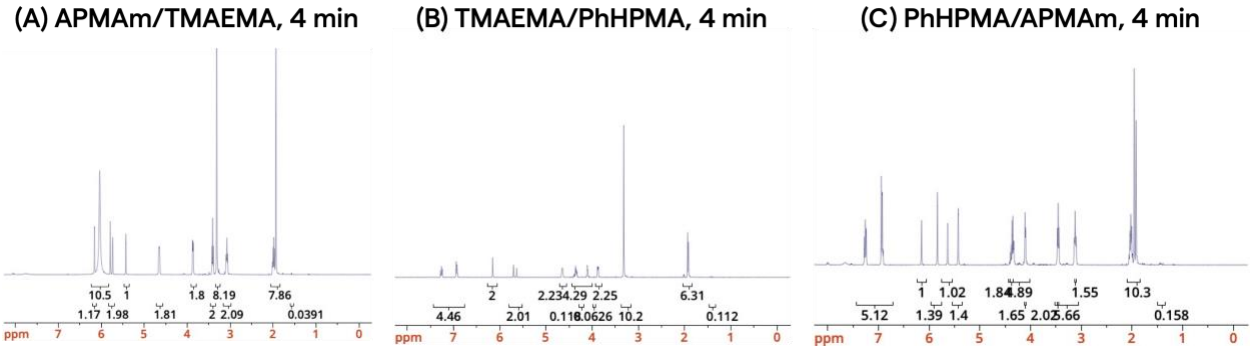

Figure S-2. ^{1}H NMR of the crude material of (A) APMAm/TMAEMA, (B) TMAEMA/PhHPMA, and (C) PhHPMA/APMAm targeted 50/50 composition at 4 min.

Tables S-1 through S-3 show the experimental run data for experiment. This contains the actual feed ratio, total monomer conversion, and calculated polymer ratio. The monomer and polymer compositions are plotted as Mayo-Lewis plots in Fig. S-3. The nonlinear fit $F_1 = (r_{12} f_1^2 + f_1 f_2) / (r_{12} f_1^2 + 2f_1f_2 + r_{21}f_2^2)$ was applied to each data set to determine the pairwise reactivity ratios. This is shown by the red curve fitted to the black open circle data points. For future, larger reactivity ratio measurement efforts, it is recommended to use an integrated copolymerization

model for higher-throughput and more accurate reactivity ratio measurement[2] and to follow new guidelines by IUPAC for determining reactivity ratios from composition data.[3]

Table S-1. Experimental runs for determining APMAm/TMAEMA reactivity ratios.

Run	Feed Ratio APMAm:TMAEMA	Total Monomer Conversion (%)	Polymer Ratio APMAm:TMAEMA
1	25:75	11.7	44:56
2	50:50	15.3	56:44
3	77:23	6.9	68:32

Table S-2. Experimental runs for determining TMAEMA/PhHPMA reactivity ratios.

Run	Feed Ratio TMAEMA:PhHPMA	Total Monomer Conversion (%)	Polymer Ratio TMAEMA:PhHPMA
1	23:77	5.3	46:54
2	51:49	7.2	52:48
3	71:29	14.9	72:28

Table S-3. Experimental runs for determining PhHPMA/APMAm reactivity ratios.

Run	Feed Ratio PhHPMA:APMAm	Total Monomer Conversion (%)	Polymer Ratio PhHPMA:APMAm
1	21:79	5.5	26:74
2	44:56	6.2	45:55
3	67:33	18.0	77:23

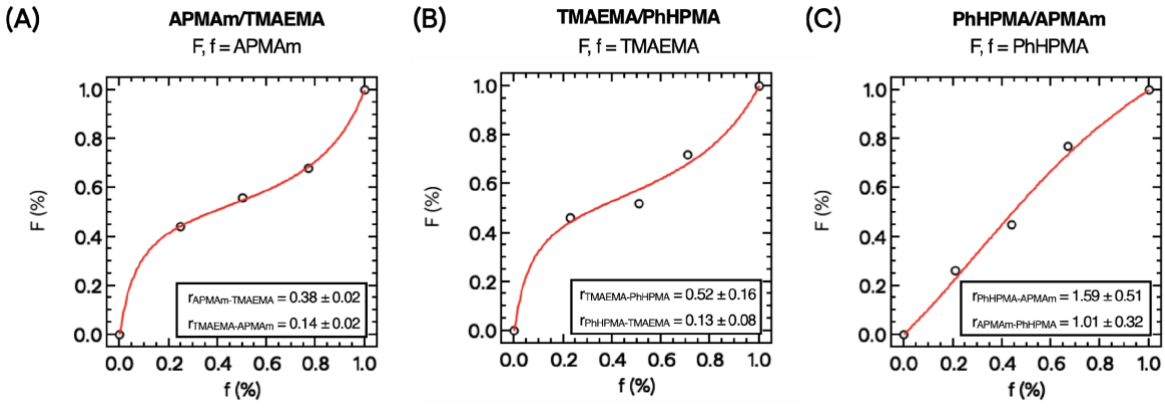

Figure S-3. Reactivity ratio determination of (A) APMAm/TMAEMA, (B) TMAEMA/PhHPMA, and (C) PhHPMA/APMAm experimental data (black open circles) with a nonlinear fit $F_1 = (r_{12} f_1^2 + f_1 f_2) / (r_{12} f_1^2 + 2 f_1 f_2 + r_{21} f_2^2)$ (red line). Error bars denote the standard deviation of the fit.

3. Polymer Characterization

Figures S-4 and S-5 show representative polymer characterization for P6 by aqueous size-exclusion chromatography and ^{1}H NMR spectroscopy, respectively. In the RI trace, the peaks right of the main polymer peak (at 20 mL, overlapping with the UV trace) are solvent signatures. We believe that the slight tailing in the main peak is a result of minor column interactions. There may also be trace nonfunctional PEG from CTA2.

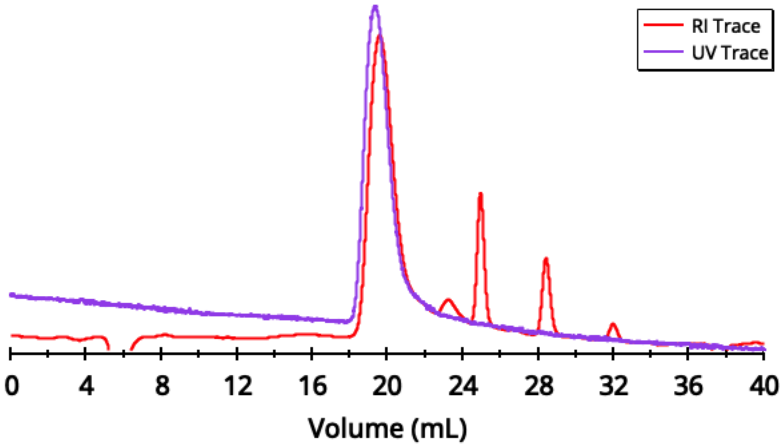

Figure S-4. Representative size-exclusion chromatogram of P6 in aqueous mobile phase (0.1 M NaH_2PO_4 + 1.0 wt % acetic acid) showing the RI (red) and UV (purple) detectors.

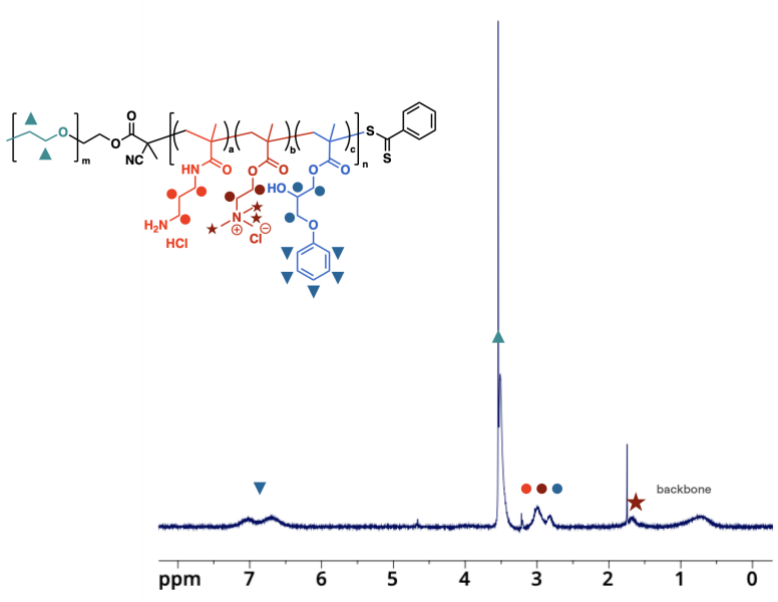

Figure S-5. Representative ^{1}H NMR of P6 in D_2O.

4. Dynamic Light Scattering Analysis

As a control, dynamic light scattering (DLS) results of PNP1 to PNP6 without salt (0 mM NaCl) are shown in Table S-4 and Figs. S-6 and S-7. N/P = 5.

Table S-4. Summary of DLS size and PDI analysis for PNPs at 0 mM NaCl.

Sample ID	R_h (nm) Cumulant	PDI Cumulant	R_h (nm) Regularization
PNP1	124	N/A	9, 76, 314
PNP2	55	0.18	53
PNP3	78	0.12	70
PNP4	36	0.16	36
PNP5	39	0.18	48
PNP6	55	0.21	54

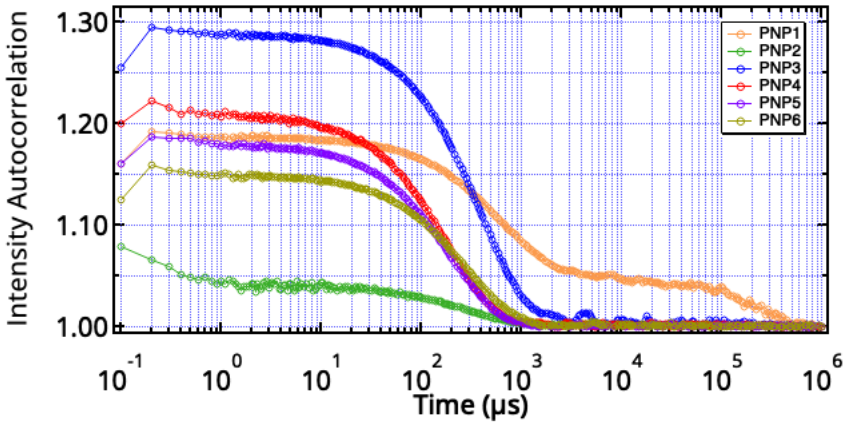

Figure S-6. Representative mean autocorrelation function for PNP1-1PNP6 in water at 25 °C.

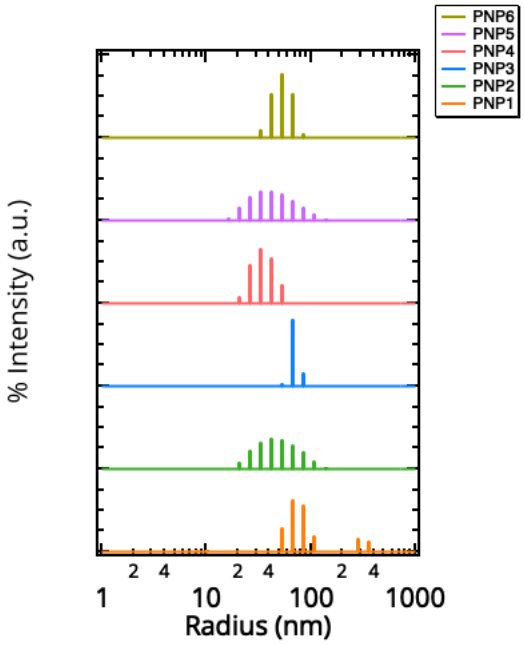

Figure S-7. Representative mean apparent size hydrodynamic radius (R_h) distribution of the PNP1-PNP6 in water at N/P = 5 at 25 °C. Calculated using regularization analysis.

Non-PEGylated PNPs are prone to swelling and aggregation as a function of added salt.[4-6] This is attributed to how changes in salinity result in responsive behavior of the polyelectrolyte phase. Often, this can be observed as aggregation from breaking intrinsic ion pairs[4] and the change in osmotic pressure between complex and supernatant phases,[5] though exceptions (PNP tightening from water expulsion) to this exist depending on polymer and salt types.[6] To examine this further, DLS screens were performed on PNP1 to PNP6 under the solution conditions outlined in Table S-5. After transferring each solution to form complexation, each well plate was immediately transferred to the instrument for data collection set at 25 or 35 °C.

Table S-5. Design matrix for solution-state polymer nanoparticle size analysis.

		NaCl		
		50 mM	100 mM	250 mM
Glucose	**0%**			
	5%			
	10%			
50 mM $CaCl_2$	**0% Glucose**			
	5% Glucose			
	10% Glucose			
100 mM $CaCl_2$	**0% Glucose**			
	5% Glucose			
	10% Glucose			

Representative autocorrelation functions (ACFs) of PNP3 and PNP6 are shown in Fig. S-8. Regularization was also applied to spot check size distributions that were not monomodal. In many cases, the addition of salt resulted in multimodal size populations. Fig. S-9 shows representative size distributions of PNP3 and PNP6 at 0, 100, and 250 mM added NaCl at 25 °C using regularization analysis. As NaCl concentration increases, the non-PEGylated PNP3 shows aggregation and broadening of PNP size. By comparison, the PEGylated PNP6 analog shows relatively robust stability with increased NaCl.

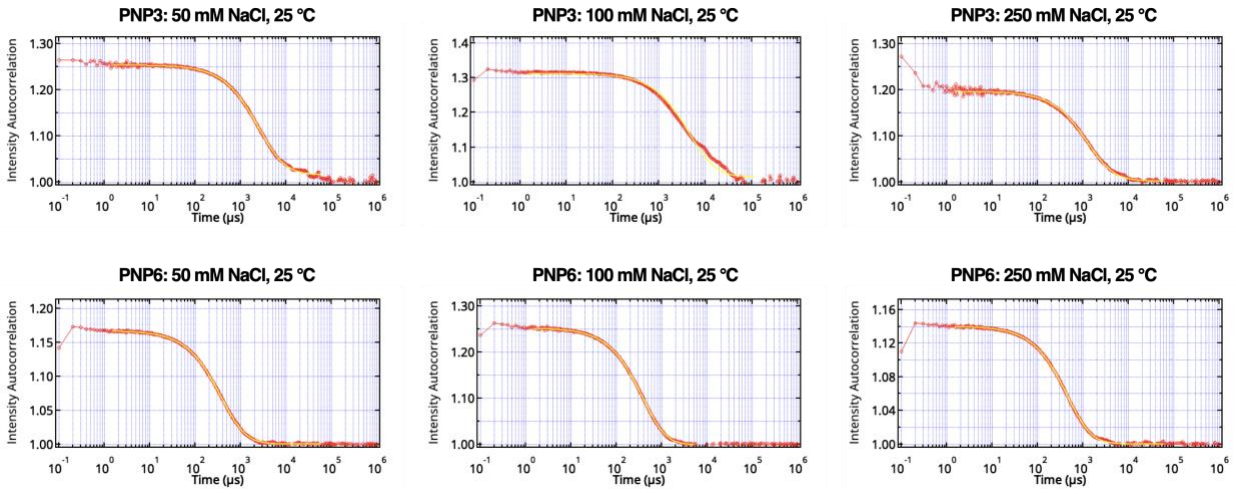

Figure S-8. Representative mean autocorrelation function for PNP3 and PNP6 at 50, 100, and 250 mM added NaCl at 25 °C. Yellow lines show the cumulant fit to the data (red).

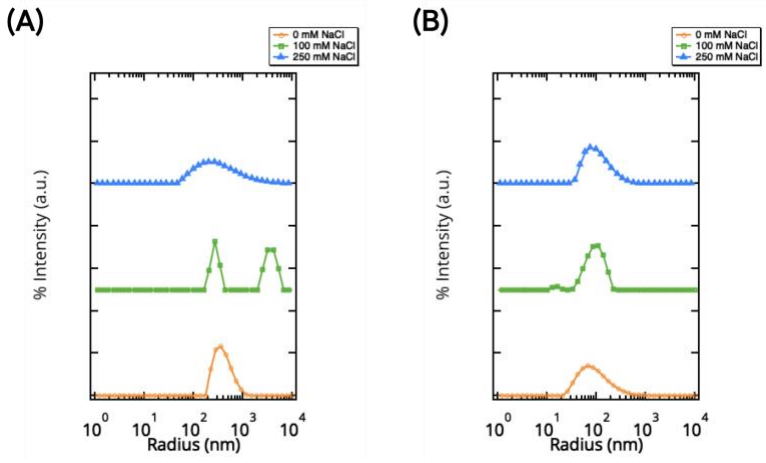

Figure S-9. Representative mean apparent size hydrodynamic radius (R_h) distribution of the (A) PNP3 and (B) PNP6 at 0 mM (orange), 100 mM (green), and 250 mM (blue) added NaCl at 25 °C (N/P = 5). Calculated using regularization analysis.

The effects of time, temperature, and sugar content were determined to be negligible for down-selecting PNP6 for *in vivo* testing. Fig. S-10 shows select results, where PNP6 shows the greatest stability under all conditions. While there are trends observed for some systems, detailed analysis remains outside the scope of this current work.

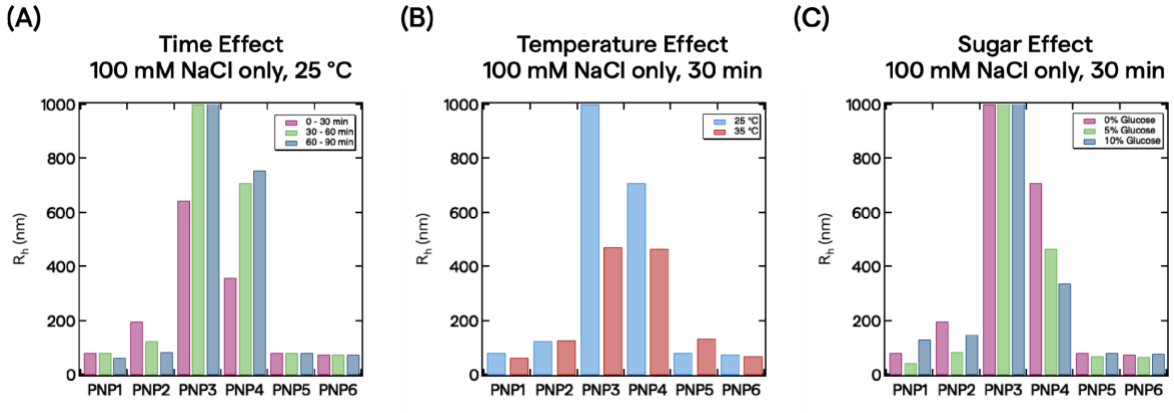

Figure S-10. Representative comparison of the (A) time, (B) temperature, and (C) sugar effects on the mean R_h of investigated PNPs. PNP3 values exceeded the general 1 μm threshold of reliability in measurement by DLS.

Figures S-11 and S-12 shows the average apparent radius (R_h) of PNP1-PNP6 under all matrix solution conditions. The polydispersity (PDI) from a cumulant fit is defined as PDI = μ_2 / Γ^2, where μ_2 is proportional to the distribution width of the ACF and Γ is the decay rate of the ACF. Note that this cannot be calculated (denoted as N/A) if a sample is multi-modal because a cumulant fit assumes a single population. These values are tabulated in Table S-6. Fig. S-13 shows the PDI values of P2 to P6 as a function of added NaCl salt concentration at 25 °C. Of these samples, PNP 6 exhibits the lowest calculated PDI.

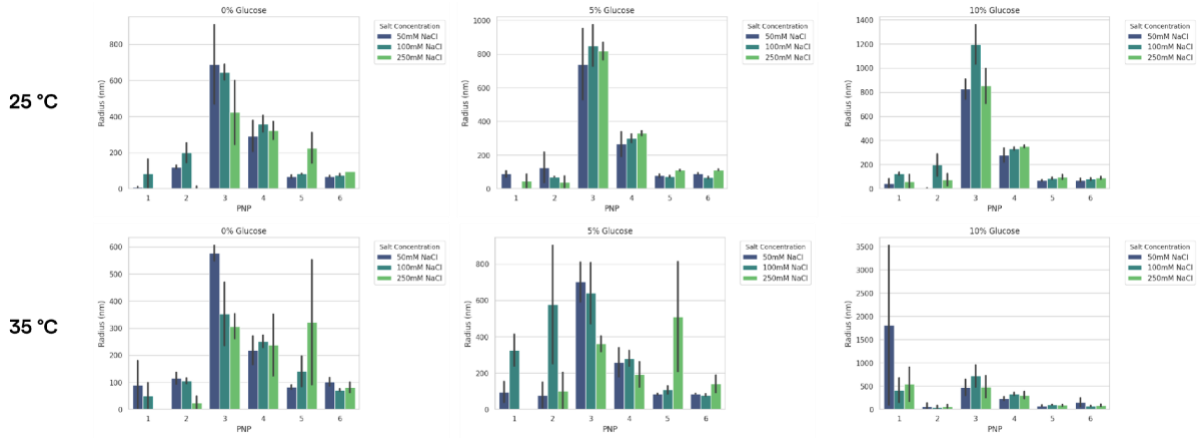

Figure S-11. Gallery of the apparent radius (R_h) of PNP1-PNP6 with 50, 100, and 250 mM added NaCl at 0, 5, and 10% added glucose at 25 and 35 °C. All values show the mean + standard deviation of 15 acquisitions from dynamic light scattering.

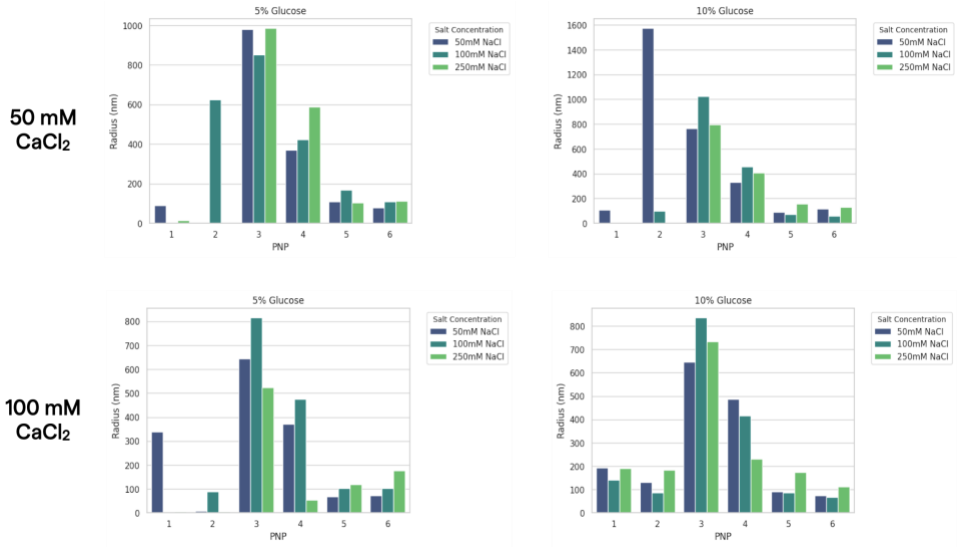

Figure S-12. Gallery of the apparent radius (R_h) of PNP1-PNP6 with 50, 100, and 250 mM added NaCl at 5 and 10% added glucose at 50 and 100 mM added $CaCl_2$ at 25 °C. All values show the mean + standard deviation of 15 acquisitions from dynamic light scattering.

Table S-6. Polydispersity values of PNPs at 25 °C.

	NaCl			
Sample	**0 mM**	**50 mM**	**100 mM**	**250 mM**
PNP1	multimodal	multimodal	multimodal	multimodal
PNP2	0.18	multimodal	multimodal	multimodal
PNP3	0.12	multimodal	multimodal	multimodal
PNP4	0.16	0.437	multimodal	multimodal
PNP5	0.18	0.409	multimodal	0.397
PNP6	0.21	0.425	0.309	0.366

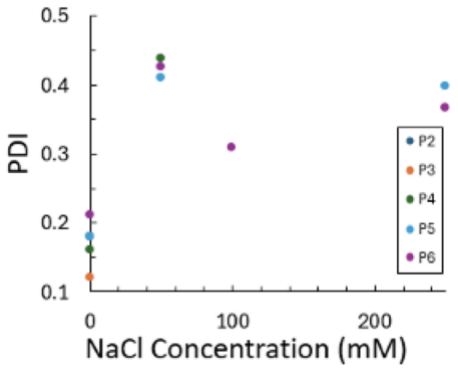

Figure S-13. Polydispersity (PDI) values of P2 to P6 as a function of NaCl salt concentration at 25 °C.

5. qPCR Detailed Methodology and Tissue Analysis

In quantitative polymerase chain reaction (qPCR) assays, data is collected throughout the process to monitor amplification of DNA. Fig. S-14-A shows the mechanism of the probe-based qPCR strategy used. This method enables detection of a specific product using a fluorogenic probe, designed with a specific binding sequence: the fluorophore emits a signal, and the quencher prevents fluorescence until replication occurs. The higher starting quantity of the target, the faster the increase in fluorescence is observed. In general, a *housekeeping gene* is used as a control, and a *target gene* is used to analyze expression.

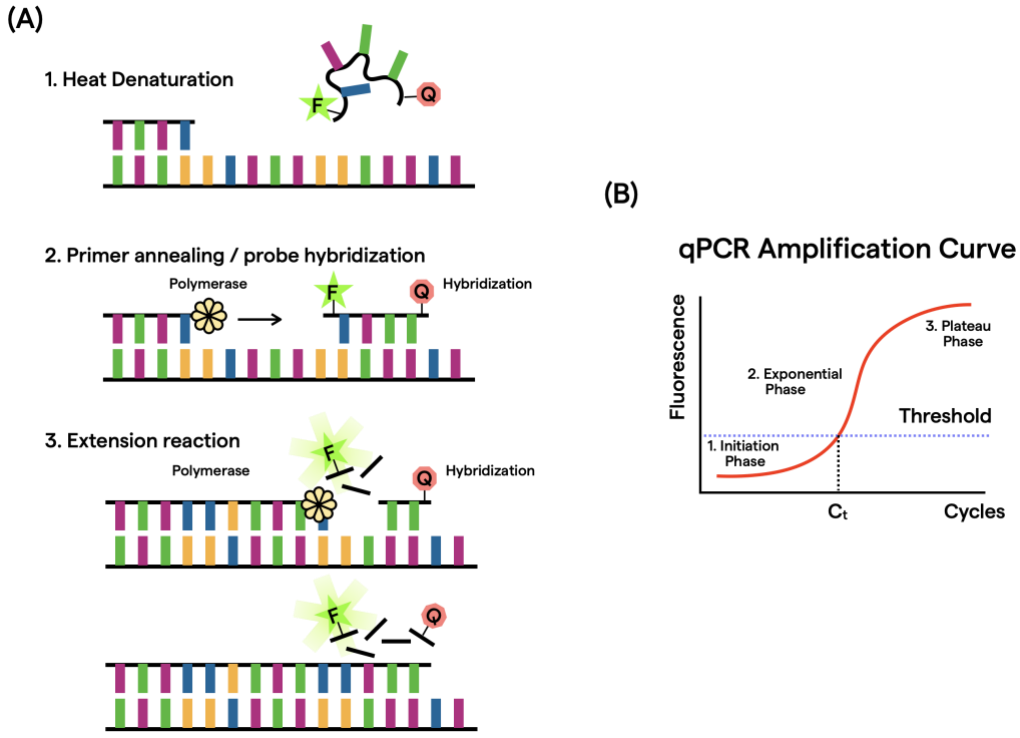

Figure S-14. (A) Reaction schematic of TaqMan-based qPCR showing the heat denaturation, primer annealing / probe hybridization, and extension reaction steps of the process. (B) Illustrative representation of a qPCR amplification curve, showing the initiation, exponential, and plateau phases of the cycle.

Fig. S-14-B provides a diagrammatic visual of a qPCR amplification curve. As replication continues, fluorescence increases as more fluorescent probes are separated from quenchers. Here, C_T is the cycle in which a threshold amount of fluorescence is reached. Thus, ΔC_T is the difference between the C_T values of the signal and housekeeping control; $-\Delta\Delta C_T$ is the difference between the ΔC_T values of the experiment and the control, normalized so that a higher signal corresponds to a higher (more positive) readout value. More information about qPCR can be found on vendors' websites like Bio-Rad.[7]

Figs. S-15 and S-16 show the calculated $-\Delta\Delta C_T$ values from animal organs from qPCR assays and the lung over liver biodistribution (defined as the difference between $-\Delta\Delta C_T$ values), respectively. The … Fig. S-17 show…

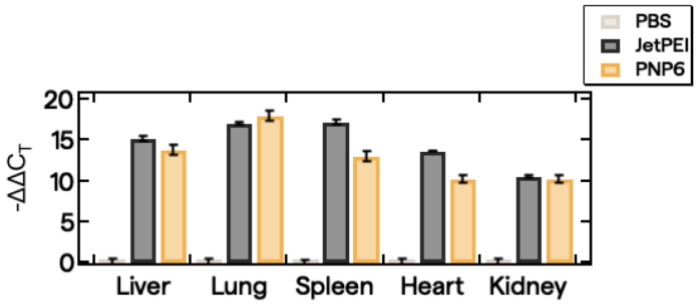

Figure S-15. Delivery of PNP6 *in vivo*. Biodistribution data of PBS (light gray), JetPEI (dark gray), and PNP6 (orange) in major organs (liver, lung, spleen, heart, and kidney) by $-\Delta\Delta C_T$ in mice. All values show the mean + standard error of the mean for N = 3 (PBS, JetPEI) or N = 4 (PNP6).

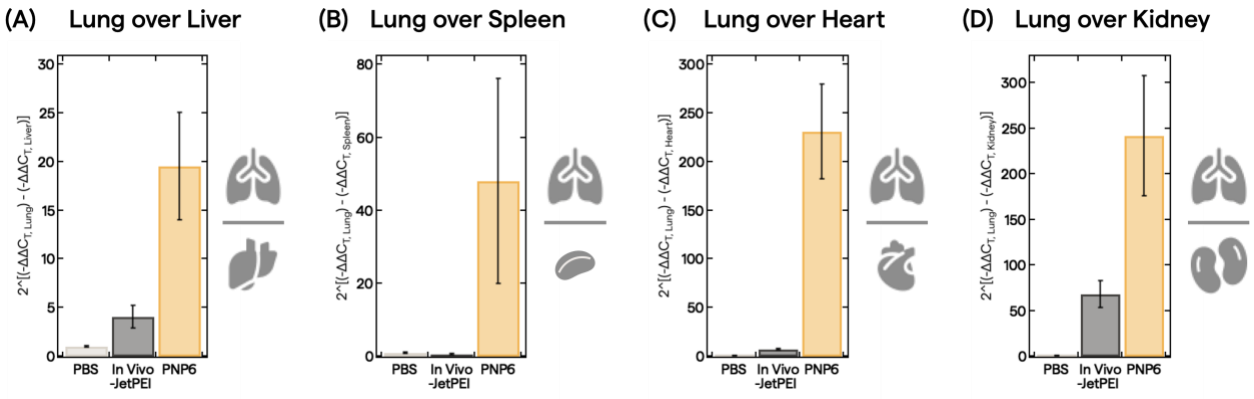

Figure S-16. Evaluation of biodelivery with the 2^(-ΔΔC_T) method by taking the mean difference between the -ΔΔC_T lung and the -ΔΔC_T of the (A) liver, (B) spleen, (C) heart, and (D) kidney values for PBS, JetPEI, and PNP6.

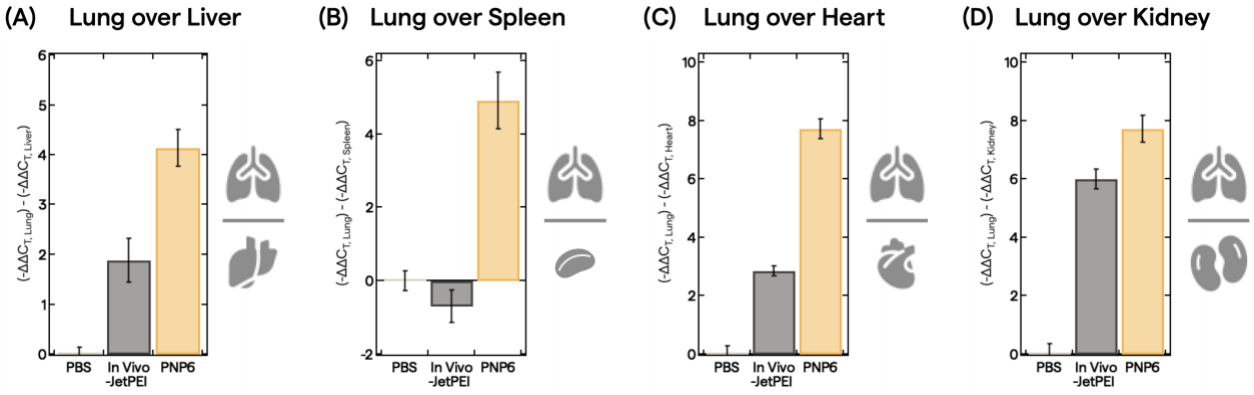

Figure S-17. Evaluation of biodelivery by taking the mean difference between the -ΔΔC_T lung and the -ΔΔC_T of the (A) liver, (B) spleen, (C) heart, and (D) kidney values for PBS, JetPEI, and PNP6.

6. *In Vitro* Transfection Evaluation

We conducted a small *in vitro* assay of the prepared polymers to (1) demonstrate the ability of PNPs to transfect EGFP protein in HEK293T cells and (2) evaluate cytotoxicity at a range of N/P ratios from 1.25 to 40. We routinely perform high-content cellular imaging and analysis using an Operetta CLS, which is capable of high-throughput live-cell microplate assays using spinning disk confocal optics Fig. S-18-A shows a representative image gallery of HEK293T cells, where green cells denote transfected cells. Fig. S-18B shows quantitative analysis of the aggregated collection of images through a heat map of the effective transfection efficiency (mean value followed by the standard error of the mean in parentheses). This is defined as the product of the mean transfection efficiency and mean cell viability, shown in Figs. S-19-A and S-19-B respectively.

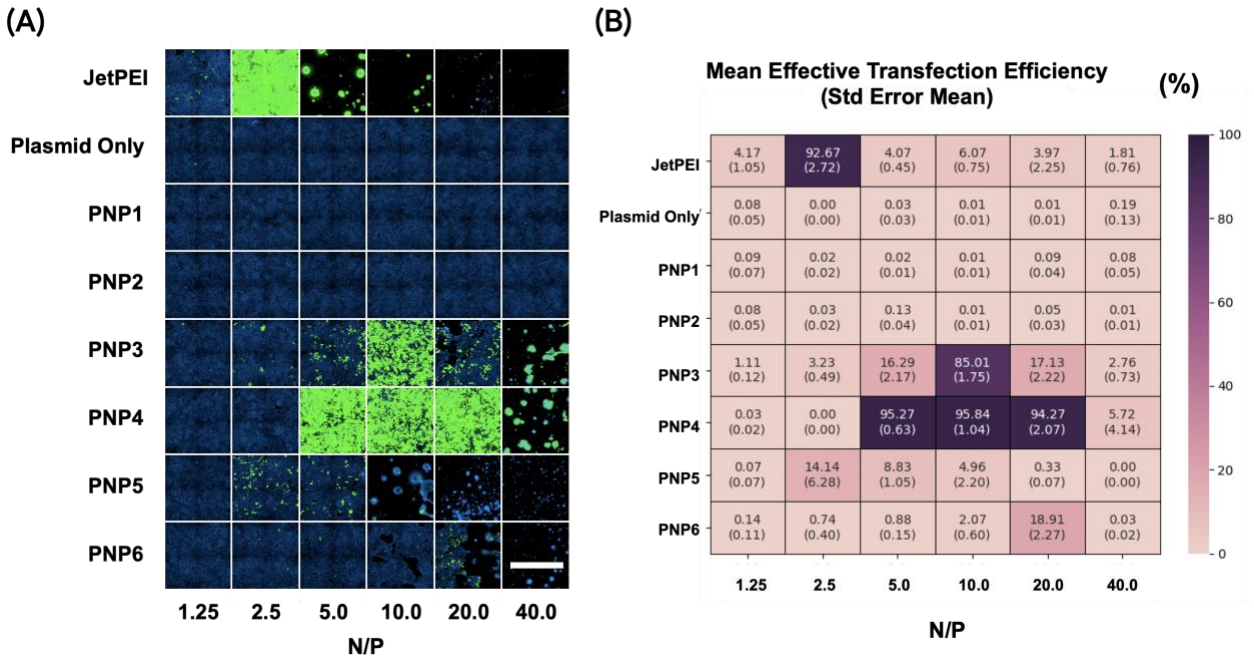

Figure S-18. (A) Image gallery of HEK293T cells transfected with investigated PNPs at N/P values from 1.25 to 40. EGFP expression and cell nuclei are visualized by green and blue (Hoechst 33342), respectively. Scale bar represents 1 mm. (B) Heat map of the mean effective transfection efficiency (defined as the product of the mean transfection efficiency and mean cell viability) across N/P = 1.25 to 40 for investigated systems.

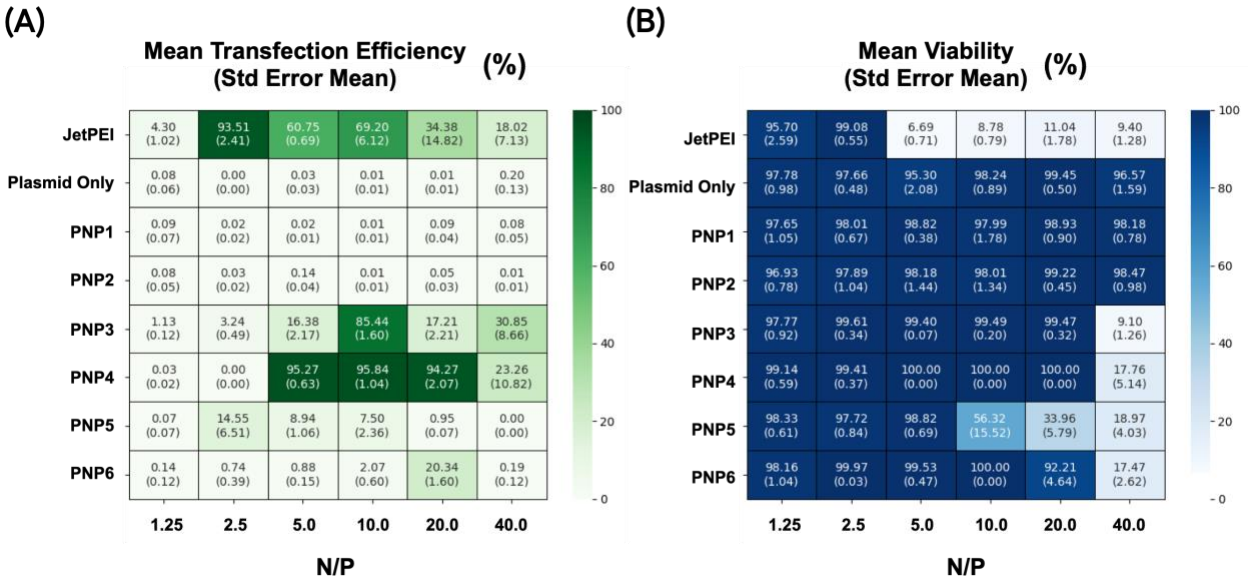

Figure S-19. Heat maps of cell (A) mean transfection efficiency and (B) mean viability across N/P = 1.25 to 40 for investigated systems.

We observe high effective transfection of the commercial positive control JetPEI (93%) . As demonstrated across the polymeric gene therapy literature,[8] at N/P > 5 formulations comprising more added polymer exceptionally high cytotoxicity is observed as the mean cellular viability drops to <10%. Among the non-PEGylated samples (PNP1, PNP2, PNP3), we only observe transfection in PNP3 (85% at N/P = 10). Solubility issues in PNP1 and PNP2 likely contributed to limited response compared to the PEGylated analogs PNP4 and PNP5. Among the PEGylated samples (PNP4, PNP5, PNP6), we observe that higher APMAm composition corresponded to higher cellular transfection. While we observe remarkably high transfection in PNP4, we attribute this in part to larger PNP size (Figs. 3, S-11, and S-12) under all conditions, which is known to be a critical feature for *in vitro* performance.[8-9] A comparison of bioperformance between PNP5 and PNP6 reveals greater viability of PNP6 with similar levels of transfection (20%) at a higher N/P of 20.

7. References

1. G. Lee, S. Kim, J. Kim, and S.-T. Yun. MEDIAR: Harmony of Data-Centric and Model-Centric for Multi-Modality Microscopy. arXiv:2212.03465. https://github.com/Lee-Gihun/MEDIAR/tree/main

2. N. A. Lynd, R. C. Ferrier Jr., and B. S. Beckingham "Recommendation for Accurate Experimental Determination of Reactivity Ratios in Chain Copolymerization" *Macromolecules* 2019, **52**, 2277–2285.

3. Autzen, A. et al. "IUPAC recommended experimental methods and data evaluation procedures for the determination of radical copolymerization reactivity ratios from composition data" *Polym. Chem.* 2024, *Advance Article*. DOI: 10.1039/D4PY00270A

4. S. L. Perry, Y. Li, D. Priftis, L. Leon, M. Tirrell "The Effect of Salt on the Complex Coacervation of Vinyl Polyelectrolytes" *Polymers*, 2014, **6**, 1756–1772.

5. S. Meng, J. M. Ting, H. Wu, M. V. Tirrell "Solid-to-Liquid Phase Transition in Polyelectrolyte Complexes" *Macromolecules*, 2020, **53**, 7944–7953.

6. H. M. Fares, Q. Wang, M. Yang, J. B. Schlenoff "Swelling and Inflation in Polyelectrolyte Complexes" *Macromolecules*, 2019, **52**, 610–619.

7. Bio-Rad. "qPCR Amplification" www.bio-rad.com/en-us/applications-technologies/qpcr-amplification?ID=3edb4096-4520-87be-7382-9bd9c130e419 (accessed Apr. 24, 2024).

8. R. Kumar, C. F. Santa Chalarca, M. R. Bockman, C. V. Bruggen, C. J. Grimme, R. J. Dalal, M. G. Hanson, J. K. Hexum and T. M. Reineke, "Polymeric Delivery of Therapeutic Nucleic Acids" *Chem. Rev.*, 2021, **121**, 11527–11652.

9. W. T. Godbey, K. K. Wu, and A. G. Mikos, “Size matters: Molecular weight affects the efficiency of poly(ethylenimine) as a gene delivery vehicle” *J. Biomed. Mater. Res.*, 1999, **45**, 268–275.